If $\mathbf{x}_1$ is reset using Eq. (49), then a similar type of reset must be applied to $\hat{\mathbf{x}}_1(t)$ at the same time. That is

$$\hat{\mathbf{x}}_1'(t) = \hat{\mathbf{x}}_1(t) - \Gamma\hat{\mathbf{x}}_1(t) \triangleq \Delta\hat{\mathbf{x}}_1(t) \tag{50}$$

In this section the effect of this type of control on the covariance matrices used in the suboptimal filter evaluation will be discussed. This is best done by rewriting Eq. (49) as

$$\mathbf{x}_1'(t) = \Gamma(\mathbf{x}_1(t) - \hat{\mathbf{x}}_1(t)) + \Delta\mathbf{x}_1(t) \tag{51}$$

The definitions of P, X, Y, U, V, and W may be used to derive the relationships between the covariance, before and after the reset. The expression relating X' to the original covariance elements as well as Γ and Δ will be derived here.

Following the definition of X in Eq. (40)

$$X = E[(\mathbf{x}_1 - \hat{\mathbf{x}}_1)x_1{}^T] \tag{40}$$

it is logical to define X' as

$$X' = E[(\mathbf{x}_1' - \hat{\mathbf{x}}_1')^T\mathbf{x}_1'^T] \tag{52}$$

However, if Eq. (50) is subtracted from Eq. (49) and the result substituted in Eq. (52), the following expression is obtained:

$$X' = E[(\mathbf{x}_1 - \hat{\mathbf{x}}_1)[\Gamma(\mathbf{x}_1 - \hat{\mathbf{x}}_1) + \Delta\mathbf{x}_1]^T] \tag{53}$$

This equation may now be expanded to yield the following relationship between X', P, X, Γ, and Δ:

$$X' = P\Gamma^T + X\Delta^T \tag{54}$$

The similar relationships for P', Y', U', V', and W' are given below.

$$P' = P \tag{55}$$

$$Y' = Y \tag{56}$$

$$U' = \Gamma P\Gamma^T + \Gamma X\Delta^T + \Delta X^T\Gamma^T + \Delta U\Delta^T \tag{57}$$

$$V' = \Gamma Y + \Delta V \tag{58}$$

$$W' = W \tag{59}$$

Equations (54–59) may be used to evaluate the effect of reset control on the performance of a system using a suboptimal filter.

References

[1] Nishimora, T., "On the a priori Information in Sequential Estimation Problems," *IEEE Transactions on Automatic Control*, Vol. AC-11, No. 4, April 1966, pp. 197–204.

[2] Sutherland, A. and Gelb, A., "Application of Kalman Filtering Aided Inertial Navigation Systems," Rept. TP 4652, Aug. 1968, Naval Weapons Center, China Lake, Calif.

[3] Stubberud, A. R. and Wismer, D. A., "Suboptimal Kalman Filter Techniques," AGARD, AD 704 306, Feb. 1970, pp. 107–117.

[4] Bobick, J. C. and Bryson, A. E., "Updating Inertial Navigation Systems with VOR/DME Information," *AIAA Journal*, Vol. 11, No. 10, Oct. 1973, pp. 1377–1384.

Thermal Analysis for Antenna Window in AGM Nosetip

JIMMIE H. SMITH*
Sandia Laboratories, Albuquerque, N. Mex.

I. Introduction

COMPUTER simulation[1, 2] of one trajectory for a current air-to-ground missile design, which includes a phenolic refrasil heat-shield nosetip, indicates that the phenolic resin binder will char and decompose to a slight extent. However, even a very thin carbonaceous char layer is electrically conductive and highly attenuating to electromagnetic signals. Thus, for flight tests with a telemetry antenna in the nose, a noncharring antenna window must be inserted. This Note describes the nosetip redesign for insertion of a noncharring antenna window and discusses the thermal considerations leading to the redesign.

Received August 16, 1973; revision received November 15, 1973. This work was done under the auspices of the U.S. Atomic Energy Commission. W. H. McCulloch assisted in the initial stage of this design task.

Index categories: Boundary Layers and Convective Heat Transfer—Laminar; Boundary Layers and Convective Heat Transfer—Turbulent; Heat Conduction.

* Staff Member, Heat Transfer Division. Member AIAA.

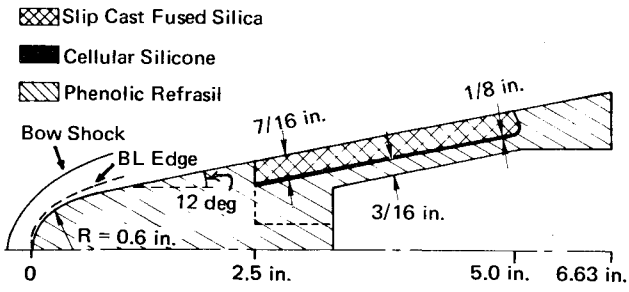

Fig. 1 AGM nosetip heat shield.

The most severe trajectories for this vehicle are similar to but less severe than the late stages of a typical re-entry vehicle flight. The operational heat shield easily meets the usual goals of: 1) low density; 2) low thermal conductivity; 3) high specific heat; 4) high resin decomposition energy; and 5) high emissivity.

To prevent charring, a slip cast fused silica antenna window designed under the following constraints was inserted in the nosetip: 1) the existing outer body contour must remain the same to preserve total missile flight parameters; 2) enough of the phenolic refrasil must remain under the slip cast fused silica to serve as structural support for underlying antenna parts; and 3) the combined thicknesses of slip cast fused silica and phenolic refrasil must remain below $\frac{3}{4}$ in. to allow sufficient volume for the antenna itself. The final design shown in Fig. 1 includes an intermediate layer of cellular silicone whose necessity will be explained later.

II. Aerodynamic Heating

The velocity of the vehicle remains within the low supersonic ($M_\infty \leq 3.5$) regime, and therefore the ionization which occurs in the inviscid flow aft of the bow shock is insignificant. The semiballistic trajectory considered here causes free-flight recovery temperatures on the order of 3000°F with forebody hot wall heating rates of about 25 Btu/ft^2-sec and integrated heat input of about 1000 Btu/ft^2. For the present problem, convective heating dominates to an extent which makes radiative heating from behind the bow shock negligible by comparison.

A code called BLUNTY[1] was selected for its fast running times and reasonably accurate predictions in keeping with knowledge of the input data. Basically BLUNTY functions as follows.

Exact inviscid flowfield solutions including shock shape and static pressure distributions over a wide range of Mach numbers are built into BLUNTY as cubic spline fits and tabular data, respectively. A streamtube mass balance is used to find boundary-layer edge properties which for equilibrium flows at zero angle of attack may be determined by entropy and pressure. The user of BLUNTY may choose between air in thermochemical equilibrium or an ideal gas. Cold wall heating rates are computed in BLUNTY with the Fay and Riddell equation[3] at the stagnation point; the Kemp, Rose, and Detra equation[4], for laminar flow; and a modification of the Rose, Probstein, and Adams equation[5] for turbulent flow.

Though almost a century has elapsed since Osborne Reynolds described boundary-layer transition, it is still the least understood of the important phenomena affecting heat-shield design.[6] Nevertheless, trial calculations indicate that assuming all-turbulent flow coupled with other conservatism leads to a

thicker heat shield than the antenna designers can tolerate. In the present work, empirical correlation data of $Re_s = \rho_e U_e S/\mu_e$ vs M_e for an aerodynamically similar phenolic refrasil heat shield is taken from the work of Martelluci and Studerus of General Electric. The wetted length from stagnation point is denoted by S. A curve fit of this data yields the following:

$$Re_s \geq \exp[10+2.5(M_e)^{1/2}] \quad (1)$$

implies fully turbulent flow for

$$1.5 \leq M_e \leq 4.5$$

The criterion is in gross agreement with the data of Gazley.[7]

III. Material Behavior

As shown in Fig. 1, the outer sheath of slip cast fused silica and the insulating layer of cellular silicone are designed to protect the phenolic refrasil from aerodynamic heating and associated pyrolysis or decomposition. The design is necessarily based on empirical determinations of material behaviour. Among the empirically determined data are: 1) temperature at which significant mass loss begins; 2) temperature and duration for complete char; and 3) residual char weight.

Because these results are a strong function of heating rate, several rates ranging from, say, 10°F/min to 100°F/min should be used. In flight, the material often undergoes heating rates of several hundred °F/min. The relative displacement of weight loss vs temperature curves for different heating rates in an inert atmosphere determines the Arrhenius decomposition constants.

For the phenolic refrasil, a low heating rate of 10°F/min causes water to exit between 200°F and 500°F and significant decomposition to begin at 500°F. To be conservative, the present heat shield is designed to keep the window-region phenolic refrasil below 400°F. Ahead of the window region, a char layer can be tolerated because dynamic pressures reach a maximum of only 8 atm at the stagnation point for a short duration. Even at the joint between the phenolic refrasil and the slip cast fused silica, recession is assumed to be small on the basis of tests performed by Mead and Sheldahl.[8]

IV. Conduction and Radiation Analyses

The cold wall reference temperature assumed for the convective heating analysis allows uncoupling of the convection equations from the transient diffusion equation for conduction in depth. The two-dimensional axisymmetric transient diffusion equation is differenced by the implicit Crank-Nicolson method with a lumped parameter grid. Radiation to space is accounted for in the source term with the usual fourth power difference.

Experimental data indicate the appropriateness of correlating hot wall heating rates in terms of a driving potential of an enthalpy difference to the first power up to much higher velocities than the maximum of 6000 ft/sec achieved here. Reinikka and Sartell[9] indicate that little error is caused by assuming that the heat transfer coefficient is independent of temperature. Further simplifications are obtained by choosing a cold wall reference temperature of $0°R$ so that $h_{cw} \equiv 0$. Also $h_r = \mathscr{R} h_s$ and $\mathscr{R} = (Pr)^{1/2}$ for laminar and $\mathscr{R} = (Pr)^{1/3}$ for turbulent flow. With the foregoing conditions, the relationship between hot and cold wall heating rates is given by Eq. (2).

$$\dot{q}_{hw} = \dot{q}_{cw}(\mathscr{R} - h_{hw}/h_s) \quad (2)$$

Equation (2) provides values for the source term in the diffusion equation as applied to surface nodes during the transient solution. In Eq. (2), subscripts denote the following: cw = cold wall; r = recovery; hw = hot wall; and s = stagnation.

V. Results and Conclusions

The first approach to the nosetip redesign included a simple $\frac{9}{16}$-in. slip cast fused silica layer outside a $\frac{3}{16}$-in. phenolic refrasil layer. Figure 2, Curve A, shows the temperatures predicted during flight with this design which was thermally satisfactory.

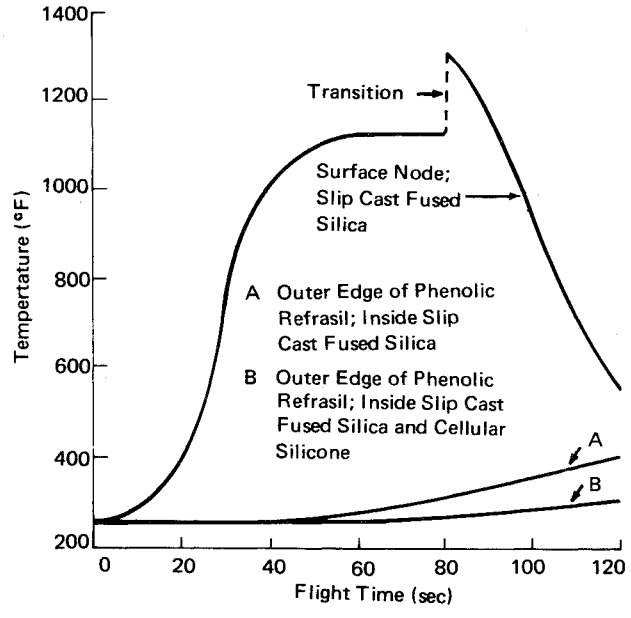

Fig. 2 Flight temperature inside antenna window with (B) without (A) insulating layer.

Unfortunately a stress prediction, to be reported elsewhere, indicated that the brass ballast in the antenna proper would expand in combination with the phenolic refrasil to an extent that would shatter the outer layer of the slip cast fused silica. A stress-mitigating layer of $\frac{1}{8}$-in. cellular silicone (see Fig. 1) solved the structural problem and provided greater conservatism thermally as shown in Fig. 2, Curve B. The nodal temperature at the window surface (also shown in Fig. 2) is the same for both configurations. Radiant heat and arcjet tests indicate the effectiveness of the present design.

The present design calculations show that mass injection into the boundary layer is small enough so that convective blockage is very small and radiative blockage is negligible. The greatest uncertainty arises from the use of an empirical boundary-layer transition criteria developed for the same material on a different vehicle. However, the conservatism given by the added insulating layer more than provides for errors in transition and hence heating rates.

References

[1] Hochrein, G. J., "A Procedure for Computing Aerodynamic Heating on Sphere Cones: Program BLUNTY," SC-DR-69-449, Nov. 1969, Sandia Labs., Albuquerque, N. Mex.

[2] Moyer, C. B. and Rindal, R. A., "Finite Difference Solution for the In-Depth Response of Charring Materials Considering Surface Chemical and Energy Balances," Final Report 66-7; Part II, March 1967, Aerotherm Corp., Mountain View, Calif.

[3] Fay, J. A. and Riddell, F. R., "Theory of Stagnation Point Heat Transfer in Dissociated Air," *Journal of the Aeronautical Sciences*, Vol. 25, No. 2, Feb. 1958, pp. 73–85.

[4] Kemp, N. H., Rose, P. H., and Detra, R. W., "Laminar Heat Transfer Around Blunt Bodies in Dissociated Air," Rept. 15, Jan. 1958, AVCO Everett Research Labs., Everett, Mass.

[5] Rose, P. H., Probstein, R. F., and Adams, M. C., "Turbulent Heat Transfer Through a Highly Cooled Partially Dissociated Boundary Layer," Rept. 14, Jan. 1958, AVCO Everett Research Labs., Everett, Mass.

[6] Morkovin, M. V., "Critical Evaluation of Transition from Laminar to Turbulent Shear Layers with Emphasis on Hypersonically Traveling Bodies," AFFDL-TR-68-149, March 1969, Wright-Patterson Air Force Base, Ohio.

[7] Gazley, C., "Boundary Layer and Transition in Subsonic and Supersonic Flow," *Journal of the Aeronautical Sciences*, Vol. 20, No. 1, 1953, pp. 19–28.

[8] Mead, K. E. and Sheldahl, R. E., "Preliminary Ablation Tests of

Dielectric Materials for Application as Radar Insulating Media," SC-TM-71-0700, Feb. 1972, Sandia Labs., Albuquerque, N. Mex.

[9] Reinikka, E. A. and Sartell, R. J., "Thermal Protection of Ballistic Entry Vehicles," *Journal of Spacecraft and Rockets*, Vol. 2, No. 4, April 1965, pp. 226–231.

Vortex-Induced Heating to Cone Flaps at Mach 6

JERRY N. HEFNER* AND ALLAN H. WHITEHEAD JR.†
NASA Langley Research Center, Hampton, Va.

EXPERIMENTAL studies[1,2] have shown that vortices, generated over the leeward surfaces of hypersonic configurations at angle of attack, can significantly influence lee-surface heating. The interaction of these vortices with the leeward surface can generate heating peaks of greater magnitude than that found in the same area at zero incidence. Localized high heating regions might be anticipated on control surfaces that protrude into the lee-side flow since these vortices could interact with the deflected control surface. The present Note discusses results of an experimental investigation conducted in the Langley 20-in. Mach 6 wind tunnel[3] to ascertain the effects of lee-side vortices on control surface heating at angle of attack. A critical feature of the experiment was an attempt to alleviate the interaction between the vortices and the control surfaces by judicious location of the control flaps.

The basic configuration was a sharp 8½° half-angle right circular cone, 30.5 cm long. Two flap configurations, each deflected into the lee-side flow 25° relative to the cone centerline, were attached to the base of the cone. One configuration used a single flap which was 3.56 cm wide and 5.08 cm long and centered about the vertical plane of symmetry. The other configuration used a pair of flaps which were each 1.78 cm wide and 5.08 cm long and mounted 1.27 cm outboard of the plane of symmetry. A flat surface, parallel with the cone centerline, extended 8.47 cm ahead of the cone base and allowed a straight hinge line for the flaps. The tests were conducted at a freestream Reynolds number based on cone length ($R_{\infty,L}$) of 7×10^6. Results for selected angles of attack (α) are presented in this Note ($\alpha = 10°$, 14°, and 20°) although the angle of attack was varied between 0° and 20°.

Surface oil flow patterns on the cone with single flap are presented in Fig. 1 to illustrate the formation of the lee-side vortices with angle of attack. Oil flow studies, not shown herein, were obtained on the cone without flaps and showed essentially the same oil flow patterns as found on the cone with the flaps. Consequently, the basic lee-surface flow phenomena are concluded to be independent of the existence of the flap. Featherlike oil smears indicate the scrubbing action of the vortices on the surface.[4] Paired lee-side vortices are generated on the upper cone surface when it is aligned with or slightly shielded from the freestream ($\alpha \simeq 8\frac{1}{2}°$–9°). At $\alpha = 10°$, these primary vortices are not well established and appear to be confined to a small region near the cone apex; however, the flow expanding around from the windward surface separates along the contour defining the flat surface ahead of the flap hinge line and forms vortices which

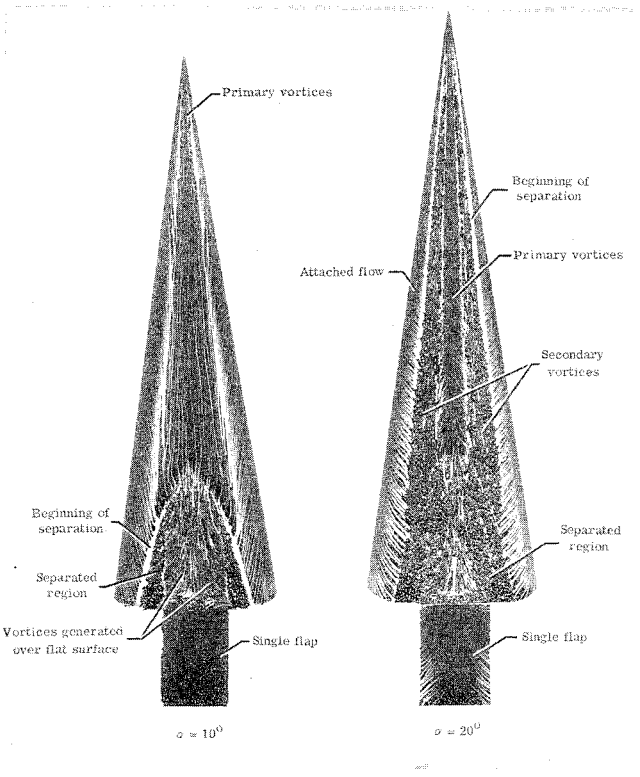

Fig. 1 Surface oil flow patterns on 8½° cone with single flap at angle of attack.

interact with the flap. As the angle of attack increases to 14° and 20°, the flow on the leeward surface separates over the entire length of the cone and the primary vortices become well established and interact more extensively with the lee surface of the cone; secondary vortices, smaller in size than the primary vortices, are generated on either side of the primary vortex pair. Unpublished schlieren photography and vapor screen studies together with the oil flow patterns indicate that although these primary and secondary vortices interact with the single flap at $\alpha = 14°$, the vortices at $\alpha = 20°$ are probably "lifted" over the flap. The interaction between the vortices and flap surface is therefore reduced at $\alpha = 20°$.

Centerline heat-transfer data obtained by the phase change paint technique[5] on the single flap are presented in Fig. 2 in

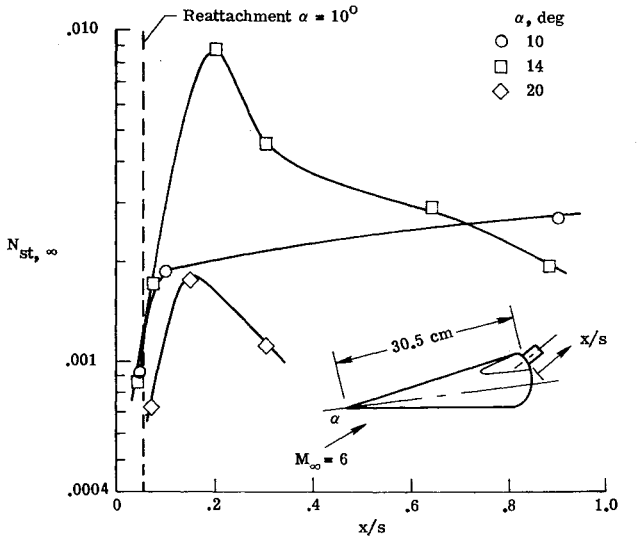

Fig. 2 Centerline heating on single flap at angle of attack.

Received August 26, 1973; revision received October 16, 1973.
Index categories: Supersonic and Hypersonic Flow; LV/M Aerodynamic Heating.

* Aerospace Engineer, Analytical Fluid Mechanics Section, Hypersonic Vehicles Division. Member AIAA.
† Technical Assistant to Director for Aeronautics. Member AIAA.